

# Electronic structure and magnetic properties of FeTe, BiFeO<sub>3</sub>, SrFe<sub>12</sub>O<sub>19</sub> and SrCoTiFe<sub>10</sub>O<sub>19</sub> compounds

G.E. Grechnev, A.A. Lyogenkaya, O.V. Kotlyar, A.S. Panfilov, and V.P. Gnezdilov  
*B. Verkin Institute for Low Temperature Physics and Engineering,  
 National Academy of Sciences of Ukraine, Kharkov 61103, Ukraine\**

The electronic energy structures and magnetic properties of iron-based compounds with group VI elements (FeTe, BiFeO<sub>3</sub>, SrFe<sub>12</sub>O<sub>19</sub> and SrCoTiFe<sub>10</sub>O<sub>19</sub>) are studied using the density functional theory (DFT) methods. Manifestations of different types of chemical bonds in magnetism of these compounds are studied theoretically. Calculations of electronic structures of these systems were performed using the generalized gradient approximation (GGA) for description of the exchange and correlation effects within DFT. For SrFe<sub>12</sub>O<sub>19</sub> and SrCoTiFe<sub>10</sub>O<sub>19</sub> hexaferrites the GGA+*U* method was also employed to deal with strongly correlated 3*d*-electrons. The calculations have revealed distinctive features of electronic structure of the investigated iron-based compounds with strongly correlated 3*d*-electrons, which can be responsible for their peculiar structural and magnetic properties.

## INTRODUCTION

The iron-based compounds are usually regarded as strong magnetic materials. However, recently the new class of iron-based superconductors was discovered. The representatives of this class are iron-based compounds with group VI elements, FeS, FeSe and FeTe, which are distinguished by the simplest crystal structure among iron-based superconductors, and very different magnetic properties [1–6]. The characteristic feature of these compounds is interplay of antiferromagnetism (AFM) and superconductivity.

Compounds of iron with another element of group VI, oxygen, are predominantly belong to ferromagnetic materials. There is renewed interest in properties of such iron oxides as BiFeO<sub>3</sub>- and MFe<sub>12</sub>O<sub>19</sub>- based systems [7–15]. BiFeO<sub>3</sub> is antiferromagnetic and multiferroic, whereas MFe<sub>12</sub>O<sub>19</sub> (*M* = Sr, Ba, Pb) are ferrimagnetic systems with expected manifestation of multiferroic properties. In these compounds a substitution of Fe or the cations with other metals can provide a mixed valence state and very unusual magnetic properties.

Clarification of microscopic mechanisms which determine electric and magnetic properties of these oxides and chalcogenides, assumes detailed theoretical studying of the electronic structure. A number of electronic structure calculations were carried out for these systems in recent years, however data on their electronic energy structure are still incomplete and inconsistent. Also, the electronic states of these systems are regarded as strongly correlated, and a proper approach has to be taken for theoretical studies of the electronic structures.

The purpose of this paper is to provide a reliable picture of the electronic band structures and corresponding magnetic properties of FeTe, BiFeO<sub>3</sub>, SrFe<sub>12</sub>O<sub>19</sub> and SrCoTiFe<sub>10</sub>O<sub>19</sub> compounds. Our study is based on the density functional theory (DFT) methods, with employing modern extensions to take into account effects of cor-

relations.

## DETAILS OF ELECTRONIC STRUCTURE CALCULATIONS

The self-consistent calculations of electronic structures were carried out by using the modified relativistic LMTO method with a full potential (FP-LMTO, RSPt implementation [16–18]) and the linearized augmented plane waves method with a full potential (FP-LAPW, Elk implementation [19]). Exchange and correlation potentials were treated within the generalized gradient approximation (GGA [20]) of DFT. Spin-orbit coupling was included in the self-consistent calculations.

For the employed full potential FP-LMTO and FP-LAPW methods any restrictions were not imposed on charge densities or potentials of studied systems, that is especially important for anisotropic layered structures of the investigated compounds. In both methods the dual basis set was employed to incorporate two valence wave functions with the same orbital quantum number (e.g. 3*p* and 4*p* functions for Fe). Electronic structure calculations for compounds were carried out for experimental crystal lattice parameters.

## ELECTRONIC STRUCTURE AND MAGNETIC PROPERTIES OF FeTe

At temperatures above 70 K FeTe compound possesses the tetragonal PbO-type crystal structure (space group *P4/nmm*). With decreasing temperature, at *T* ≈ 70 K, FeTe demonstrates a first-order structural phase transition from tetragonal to monoclinic structure. This transition is accompanied by bicollinear AFM ordering, as determined by means of x-ray and neutron diffraction studies [1–4], and we used the experimental data on structural parameters *a*, *b* and *c* in our calculations. The angle be-

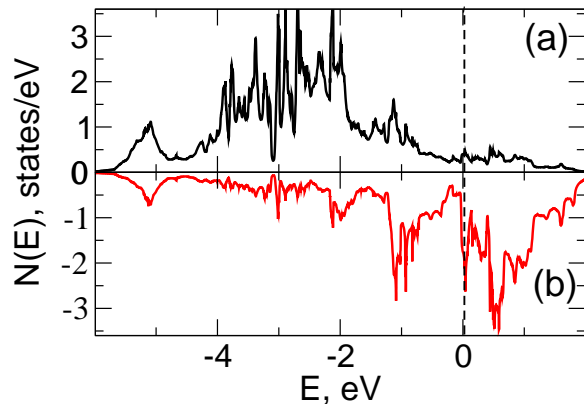


FIG. 1: (Color online) Spin-polarized densities of states  $N(E)$  of FeTe compound for the double-stripe AFM phase (per formula unit): positive ((a), black) and negative ((b), red) values of DOS correspond to majority and minority spin states, respectively. The position of Fermi level ( $E_F = 0$ ) is marked by a vertical dashed line.

tween axes was taken as  $90^\circ$  (instead of  $89.2^\circ$  for the actual structure with small monoclinic distortion).

The calculations of electronic structure were carried out in the GGA-approximation for magnetic phases of FeTe (ferromagnetic, collinear AFM, bicollinear AFM) and it was demonstrated, that minimum of total energy is found for the bicollinear (or “double stripe”, DS) AFM phase, which appears to be a ground state of FeTe compound. The calculated for the ground state spin-polarized densities of electronic states (DOS) are presented in Fig. 1. As can be seen in Fig. 1 (b), in the DS AFM phase of FeTe the Fermi level is located in very close proximity ( $\sim 0.1$  eV) of the sharp peak of DOS.

The spin-polarized splitting of DOS  $N(E)$  (see Fig. 1) provides formation of magnetic moments at Fe sites for DS AFM phase of FeTe. The obtained in our calculations value of the magnetic moment  $M_{\text{Fe}} \cong 2.37\mu_B$  is in agreement with the results of neutron diffraction studies ( $M_{\text{Fe}}^{\text{exp}} = 2.26 \div 2.54\mu_B$  [2, 4]). Such good agreement with experiment confirms the itinerant nature of magnetic moments in FeTe and adequacy of DFT–GGA approximation which we used in the present calculations of magnetic characteristics. The calculated spin density contours in the (001) plane for the AFM phase of FeTe compound are presented in Fig. 2. The double stripe structure of the ground state AFM phase is clearly seen in this figure.

The calculated charge density contours in the vertical (100) plane of unit cell of FeTe compound are presented in Fig. 3. It demonstrates a substantial anisotropy of the charge density distribution between iron atom and neighbouring atoms of tellurium. It is plausible to assume, that formation of directed covalent bonds between the neighbouring Fe and Te atoms, seen in Fig. 3, is

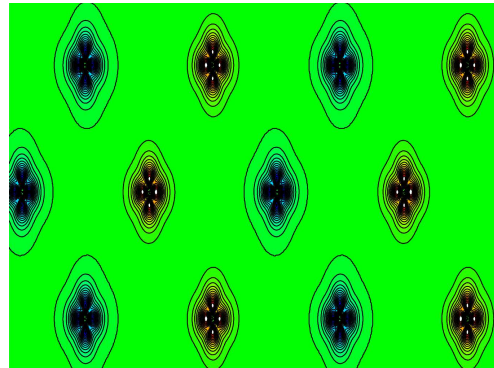


FIG. 2: (Color online) Calculated spin density contours in the (001) plane for the double-stripe antiferromagnetic phase of FeTe. (For clarification of this color figure, the reader is referred to the web version of the paper.)

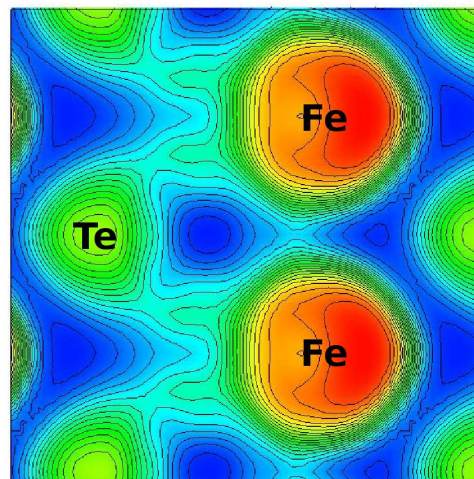


FIG. 3: (Color online) Calculated charge density contours in the (100) plane for FeTe compound in DS AFM phase. (For clarification of this color figure, the reader is referred to the web version of the paper.)

caused by hybridization of  $d$ -states of iron and  $p$ -states of tellurium.

For a more detailed study of the chemical bonds in FeTe compound, we have calculated the crystal orbital overlap populations (BCOOP, [21]) by using the FP-LMTO method [17]. The calculated BCOOP( $E$ ) distributions (see Fig. 4) represent generalization for solids of the crystal orbital overlap population (COOP) molecular characteristics, known in quantum chemistry. The values of BCOOP( $E$ ) depend on the energy of the electronic states in the valence band and are positive for bonding orbitals and negative for antibonding orbitals, as well as in the case of ionic bonding [21]. The metallic type bonding is characterized by negative values of BCOOP( $E$ ) at

energies close to the Fermi level.

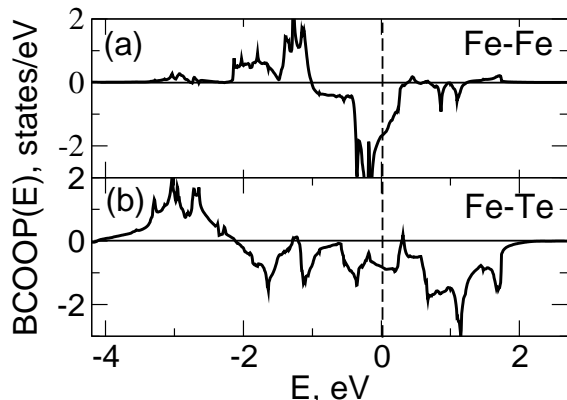


FIG. 4: Balanced crystal orbital overlap populations  $\text{BCOOP}(E)$  of FeTe compound in the DS antiferromagnetic phase for the pairs of nearest atoms in the unit cell: (a) Fe—Fe; (b) Fe—Te. The position of Fermi level ( $E_F = 0$ ) is indicated by a vertical dashed line.

According to results of  $\text{BCOOP}(E)$  calculations, the overlap of Fe—Te orbitals gives bonding states closer to the bottom of valence band (positive  $\text{BCOOP}(E)$  in the range  $-4 \div -2$  eV, see Fig. 4 (b)). The bonding states are also formed at Fe—Fe orbital overlapping in the energy range  $-3 \div -1$  eV (Fig. 4 (a)). In the vicinity of the Fermi energy, in the range  $-1 \div 1$  eV, for Fe—Te and Fe—Fe bonds the negative values of  $\text{BCOOP}(E)$  were obtained (Fig. 4 (a) and (b)), and this corresponds to a metallic type of bonding. Basically, the calculated distribution of electronic density in Fig. 3 definitely has features of metallic bonding, whereas distinct covalent bonds are formed between Fe and Te atoms.

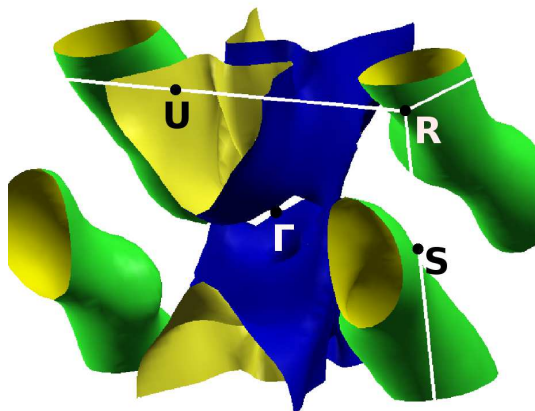


FIG. 5: (Color online) Calculated Fermi surface of FeTe compound in the bicollinear AFM phase. (For clarification of this color figure, the reader is referred to the web version of the paper.)

In this work the Fermi surface (FS) of the low-temperature DS AFM phase of FeTe was calculated for the first time, and it is presented in Fig. 5. The complicated shape of this FS differs drastically from that of paramagnetic FeTe, which was calculated earlier [22] and represents compensating electron and hole cylinders. This radical FS reconstruction at the AFM transition can be the origin of the sign reversal of the Hall coefficient which has been observed in FeTe [23]. Due to the multi-band electronic structure of FeTe, the AFM transition presumably initiates a reversal of the balance between electron and hole contributions to the Hall coefficient.

### ELECTRONIC STRUCTURE AND MAGNETIC PROPERTIES OF $\text{BiFeO}_3$

The compound  $\text{BiFeO}_3$  is a typical representative of substances known as magnetoelectrics or multiferronics, in which magnetic and electric orderings coexist. Bismuth ferrite  $\text{BiFeO}_3$  has a relatively simple crystalline structure of perovskite type and is of interest as a model object for theoretical studies of magnetic and electrical properties. In the last decade nonempirical calculations of the electronic structure were performed for different crystalline modifications of bismuth ferrite, and the importance of including Coulomb correlations in the LSDA+U or GGA+U approximations for a correct description of the electronic structure and ferroelectric properties of  $\text{BiFeO}_3$  was indicated [24–26]. On the other hand, the possibility of describing the electronic structure and magnetism of  $\text{BiFeO}_3$  within the density functional theory in the generalized gradient approximation has not been consistently and comprehensively investigated. Here we have calculated electronic structure and magnetic properties of  $\text{BiFeO}_3$  in the DFT–GGA approximation, without including the Coulomb parameter U, with the FP-LAPW method including spin-orbital coupling [19].

At low temperatures  $\text{BiFeO}_3$  has a rhombohedral distorted perovskite crystal structure (space group  $R3c$ ). The electronic structure was calculated for the experimental values of crystal lattice parameters, assuming the collinear  $G$ -type antiferromagnetic ordering [24]. The rhombohedral angle of the  $R3c$  structure was fixed at its experimental value of  $\alpha_R = 59.35^\circ$ . The calculated partial electronic densities of states (DOS)  $N(E)$  for  $\text{BiFeO}_3$  in the  $G$ -type antiferromagnetic phase are shown in Fig. 6. This figure shows that the  $G$ -type AFM phase is characterized by an insulating state with an energy gap of about 1 eV, in good agreement with emission and absorption spectroscopy data [26].

In Fig. 6 (b) one can see a narrow band at energies about  $-10$  eV originating from  $6s$ -states of Bi and hybridized with  $2p$ -states of oxygen. On the other hand, the  $6p$ -states of Bi are substantially higher in energy. It

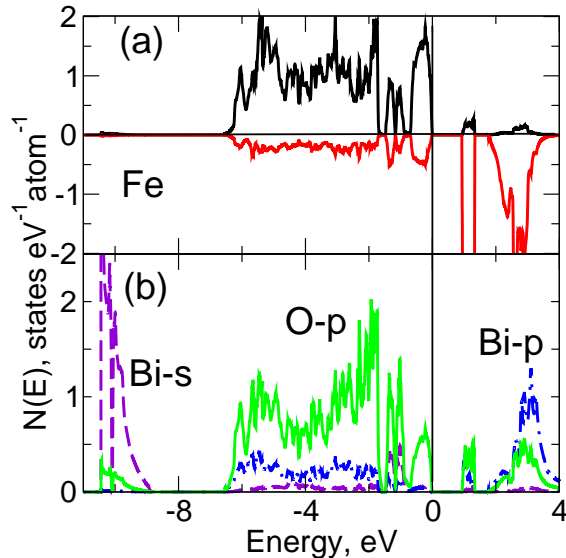


FIG. 6: (Color online) Partial densities of electronic states  $N(E)$  of  $\text{BiFeO}_3$  in the  $G$ -type antiferromagnetic phase: (a) spin-polarized densities of states per Fe atom: positive (black) and negative (red) values of DOS correspond to majority and minority spin states, respectively; (b) densities of states of  $s$ - and  $p$ -type per Bi atom: dashed (violet) and dashed-dotted (blue) curves, respectively; density of states per oxygen atom: solid green curve. The Fermi level ( $E_F = 0$ ) is indicated by a vertical line. (For clarification of the references to color in this figure caption, the reader is referred to the web version of this paper.)

can be expected that this narrow band, which is predominantly of  $6s$ -states of Bi, corresponds to so-called stoichiometrically active “lone pair” electrons, which are assumed to be responsible for polarization in ferroelectrics based on bismuth and lead [7, 8]. Due to hybridization with  $2p$ -states of oxygen, this  $6s$  “lone pair” can no longer have a purely spherical spatial charge distribution, but can acquire a component in the form of a “lobe”, which is characteristic for  $p$ -orbitals. Then, the  $\text{Bi}(s)\text{-O}(p)$  hybridization leads to a noticeable spatial anisotropy in the charge density distribution. Thus, hybridization of  $sp$ -orbitals of Bi with  $2p$ -orbitals of oxygen leads to asymmetric charge transfer in the Bi–O bonds which evidently facilitates the development of ferroelectricity.

For a more detailed study of the chemical bonds in  $\text{BiFeO}_3$ , we have calculated the crystal orbital overlap populations (BCOOP, [21]) by using the FP-LMTO method [17]. The calculated  $\text{BCOOP}(E)$  distributions (see Fig. 7) represent generalization of the crystal orbital overlap population (COOP) characteristics from quantum chemistry for solids. The values of  $\text{BCOOP}(E)$  depend on the energy of the electronic states in the valence band and are positive for bonding orbitals and negative

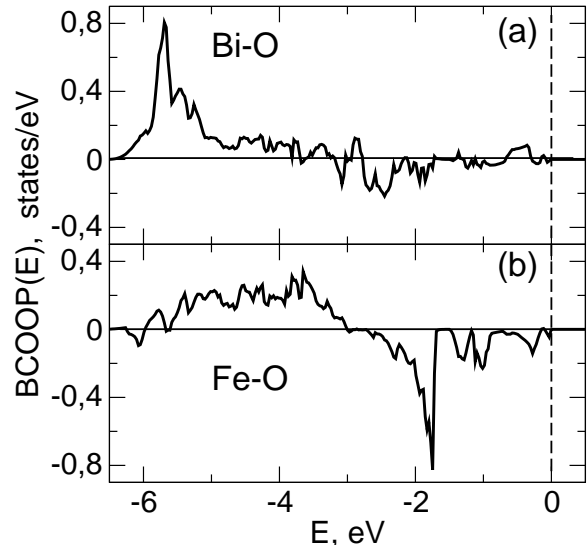


FIG. 7: Crystal orbital overlap populations  $\text{BCOOP}(E)$  of  $\text{BiFeO}_3$  in the  $G$ -type antiferromagnetic phase for the pairs of nearest atoms in the unit cell: Bi–O (a), Fe–O (b). The top of the valence band ( $E = 0$ ) is indicated by a vertical dashed line.

for antibonding orbitals, as well as in the case of ionic bonding [21].

According to the  $\text{BCOOP}(E)$  calculations, the most distinct bonding states in the valence band of  $\text{BiFeO}_3$  are formed in the  $\text{FeO}_6$  octahedra upon hybridization of  $d$ -states of iron with  $p$ -states of oxygen (Fig. 7 (b)). This is consistent with the exact coincidence in energy of the dominant regions of the partial densities of the  $d$ -states of iron (Fig. 6 (a)) and  $p$ -states of oxygen (Fig. 6 (b)) in the valence band of  $\text{BiFeO}_3$ .

Overlap of the Bi–O orbitals yields bonding states near the bottom of the valence band (positive  $\text{BCOOP}(E)$  in Fig. 7 (a)). It should be noted that the contribution of the  $p$ -states of Bi in the valence band is substantially depleted (Fig. 6 (b)) due to the charge transfer from Bi to neighbouring Fe and O atoms. This can be the origin of the ionic bonding for Bi–O orbitals in the upper part of the valence band (see Fig. 7 (a)).

On the other hand, the ionic bonding is even more pronounced for Fe–O bonds near the top of the valence band (Fig. 7 (b)). The corresponding charge transfer in Fe–O pairs provides the distortion of the  $\text{FeO}_6$  octahedra in  $\text{BiFeO}_3$  [7, 8]. In fact, our calculations indicate a predominantly ionic character of the chemical bonds in  $\text{BiFeO}_3$ . Hybridization of  $\text{Fe}(d)$ - and  $\text{O}(p)$ -states also produces a partially covalent component of the Fe–O bond.

The antiferromagnetic ordering in  $\text{BiFeO}_3$  provides the spin-split density of states  $N(E)$ , and the magnetic moments are predominantly formed at iron ions (see. Fig. 6 (a)). The calculated value of  $M_{\text{Fe}} \cong 3.7\mu_B$  agrees with data from neutron diffraction studies ( $M_{\text{Fe}} \cong 3.75\mu_B$

[27]). This good agreement with experiment supports the reliability of the DFT-GGA approach used here, which can be applied for studying magnetic properties of  $\text{BiFeO}_3$  under pressure and doping. It is also revealed, that a part of the total magnetic moment of the unit cell is distributed among neighbouring oxygen ions (up to  $0.2 \mu_B$  per O ion).

### ELECTRONIC STRUCTURE AND MAGNETIC PROPERTIES OF $\text{SrFe}_{12}\text{O}_{19}$ AND $\text{SrCoTiFe}_{10}\text{O}_{19}$

Hexaferrites  $\text{SrFe}_{12}\text{O}_{19}$ ,  $\text{BaFe}_{12}\text{O}_{19}$ , and  $\text{PbFe}_{12}\text{O}_{19}$  are known as strong permanent magnets, and have been intensively studied for the last decade due to their intriguing magnetic and chemical properties. Many efforts were undertaken to tune magnetic properties of hexaferrites by substituting  $\text{Fe}^{3+}$ ,  $\text{Ba}^{2+}$  and  $\text{Sr}^{2+}$  cations with other transition metal or rare earth ions at various lattice sites (see Refs. [10, 13–15] and references therein). Recently, the  $\text{SrFe}_{12}\text{O}_{19}$  hexaferrite was found to become magnetoelectric at room temperature by substitution of Fe with Ti and Co [14, 15]. The aim of the present investigation was, firstly, to find a reliable approach of DFT to describe properly electronic structure and magnetism of  $\text{SrFe}_{12}\text{O}_{19}$ , and then, using this approach, to explore electronic structure and magnetic properties of  $\text{SrFe}_{12}\text{O}_{19}$ -based systems where Fe is substituted with Ti and Co atoms.

Compound  $\text{SrFe}_{12}\text{O}_{19}$  possess the hexagonal crystal structure which belongs to the  $P6_3/mmc$  space symmetry group [10]. The double formula unit cell contains 64 atomic sites distributed among 11 inequivalent Wyckoff positions:  $2d$  (Sr),  $2a$  (Fe),  $2b$  (Fe),  $4f_1$  (Fe),  $4f_2$  (Fe),  $12k$  (Fe),  $4e$  (O),  $4f$  (O),  $6h$  (O),  $12k_1$  (O),  $12k_2$  (O). According to the previous studies [9, 10, 12, 13], the stable spin configuration is assumed to be ferrimagnetic with Fe at the  $4f_1$  and  $4f_2$  sites having the magnetic moment anti-parallel to the rest of the Fe cations.

It has been established, that LSDA approach has provided incorrectly metallic ground state of  $M\text{Fe}_{12}\text{O}_{19}$  hexaferrites [10, 11]. Therefore for  $\text{SrFe}_{12}\text{O}_{19}$  we firstly used DFT GGA approach [20], which usually gives more reliable picture of the ground state for systems with  $3d$ -electrons. The GGA+ $U$  approach was also employed within FP-LAPW method [19] in line with Ref. [28] for LSDA+ $U$ , but with the GGA instead of LSDA exchange-correlation potential. It is believed that this approach provides better description of electronic structure for localized electrons in the  $3d$ -transition metal oxides. The on-site Coulomb repulsion energy  $U$  was taken close to previous *ab initio* estimates [10, 13],  $U=4$  eV. The exchange parameter  $J$  was assumed to be close to its atomic value  $J \simeq 1$  eV [28].

The results of GGA and GGA+ $U$ -based calculations of DOS for  $\text{SrFe}_{12}\text{O}_{19}$  compound are presented in Fig. 8,

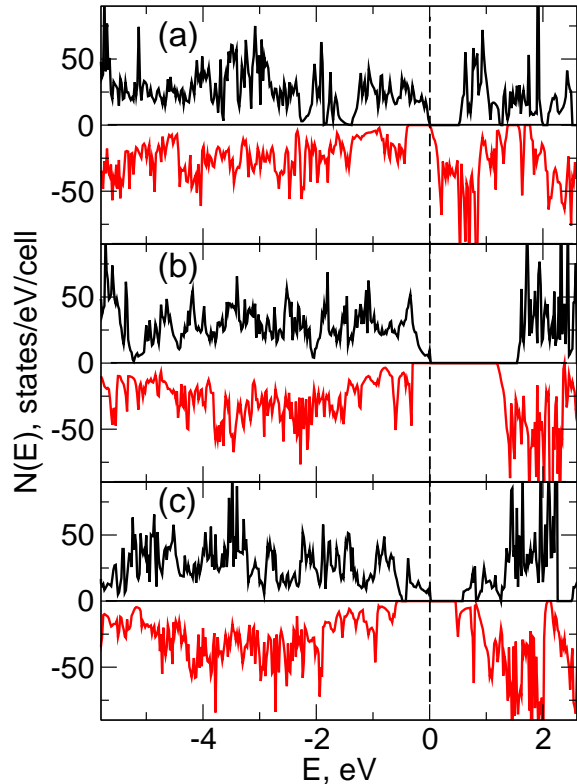


FIG. 8: (Color online) Total spin-polarized densities of electronic states of strontium hexaferrites: (a)  $\text{SrFe}_{12}\text{O}_{19}$ , GGA; (b)  $\text{SrFe}_{12}\text{O}_{19}$ , GGA+ $U$ ; (c)  $\text{SrCoTiFe}_{10}\text{O}_{19}$ , GGA+ $U$ . Positive (black) and negative (red) values of DOS correspond to majority and minority spin states, respectively. The Fermi level ( $E_F = 0$ ) is indicated by a vertical dashed line.

(a) and (b), respectively. As can be seen in Fig. 8 (a), the GGA FP-LAPW calculations for the spin-polarized ferrimagnetic state have provided the almost zero gap semiconductor. The energy gaps are enlarged in both majority and minority spin channels, which are moved apart and almost overlapped. For the GGA+ $U$  calculations the insulating ground state was obtained in agreement with experiment (see Refs. [9, 12]) with the energy gap  $E_G \simeq 1.2$  eV, as is seen in Fig. 8 (b).

The magnetic moments for all inequivalent atoms in the unit cell of  $\text{SrFe}_{12}\text{O}_{19}$ , which were calculated with both GGA and GGA+ $U$  approaches, are listed in Table I. For the insulating GGA+ $U$  case the sum of all magnetic moments per unit cell equals to  $40 \mu_B$ , which formally corresponds to  $5 \mu_B$  per Fe ion in the adopted ferrimagnetic structure. In fact, however, the theoretical value of  $5 \mu_B$  corresponding to the free  $\text{Fe}^{3+}$  ion is reduced in a crystal field environment, and a part of the total magnetic moment is transferred to neighbouring oxygen ions, as is seen in Table I. Actually, the Fe ions in  $\text{SrFe}_{12}\text{O}_{19}$  have magnetic moments close to  $4 \mu_B$ , as it comes from GGA+ $U$  calculations.

TABLE I: Local magnetic moments of ions in different Wyckoff sites of  $\text{SrFe}_{12}\text{O}_{19}$  and  $\text{SrCoTiFe}_{10}\text{O}_{19}$  calculated using GGA and/or GGA+ $U$  functionals. Magnetic moments  $M$  are given in  $\mu_B$ .

Wyckoff position	$\text{SrFe}_{12}\text{O}_{19}$			$\text{SrCoTiFe}_{10}\text{O}_{19}$	
	atom	$M$ , GGA	$M$ , GGA+ $U$	atom	$M$ , GGA+ $U$
2 <i>d</i>	Sr	-0.016	-0.018	Sr	-0.017
2 <i>a</i>	Fe	3.748	4.052	Ti	0.215
2 <i>b</i>	Fe	3.583	3.934	Co	2.604
4 <i>f</i> <sub>1</sub>	Fe	-3.490	-3.907	Fe	-3.910
4 <i>f</i> <sub>2</sub>	Fe	-3.258	-3.922	Fe	-3.911
12 <i>k</i>	Fe	3.768	4.066	Fe	4.071
4 <i>e</i>	O	0.492	0.492	O	0.497
4 <i>f</i>	O	0.142	0.123	O	0.110
6 <i>h</i>	O	0.100	0.051	O	0.069
12 <i>k</i> <sub>1</sub>	O	0.123	0.114	O	0.007
12 <i>k</i> <sub>2</sub>	O	0.217	0.218	O	0.220

The electronic structure of  $\text{SrCoTiFe}_{10}\text{O}_{19}$  compound was calculated using the GGA+ $U$  method. Following results of previous studies for 3*d*-transition metal oxides [9, 15], we used  $U = 4$  eV for Fe and  $U = 3$  eV for Co as the appropriate values for our GGA+ $U$  calculations. Based on total energy calculations, we conclude that in the ground state configuration Ti and Co ions preferentially occupy 2*a* and 2*b* positions, respectively. It should be noted, that configuration with Ti and Co ions in 12*k* and 4*f*<sub>1</sub> positions, respectively, corresponds to slightly higher total energy, and also requires consideration for the recently synthesized  $\text{SrCo}_2\text{Ti}_2\text{Fe}_8\text{O}_{19}$  multiferroic compound [15].

Our GGA+ $U$  calculations have revealed the insulating ground state for  $\text{SrCo}_2\text{Ti}_2\text{Fe}_8\text{O}_{19}$  with the energy gap  $E_G \simeq 0.5$  eV, as is seen in Fig. 8 (c). The magnetic moments on Co atoms are found to be  $2.6 \mu_B$  (see Table I), which is lower than that corresponding to a high spin state of  $\text{Co}^{2+}$  ion. As in the case of  $\text{Fe}^{3+}$  ions, the high value of the moment corresponding to free  $\text{Co}^{2+}$  ion is reduced in the crystal field, and the total magnetic moment is partly distributed among neighbouring oxygen ions, as is seen in Table I. The sum of all magnetic moments per unit cell of  $\text{SrCo}_2\text{Ti}_2\text{Fe}_8\text{O}_{19}$  equals to  $28 \mu_B$ .

## CONCLUSIONS

Results of the present GGA DFT calculations indicate predominantly metallic character of chemical bonding in FeTe compound, with partially covalent components of Fe–Te, Te–Te and Fe–Fe bonds. In fact, a hybridization of *d*-states of iron with *p*-states of tellurium results in the pronounced anisotropy of spatial distribution of charge

density in area between the planes of Fe and Te, and also in the Te→Fe charge transfer. The presence of covalent bonding presumably promotes stabilization of monoclinic structural distortions of the tetragonal phase of FeTe at low temperatures.

Results of the present calculations affirm that magnetic properties of FeTe are well described within the approach of itinerant electrons and GGA DFT. In particular, it is established that the bicollinear AFM phase has the lowest total energy, being the ground state of FeTe compound. The calculated value of magnetic moment for the bicollinear AFM phase ( $M_{\text{Fe}} \simeq 2.4\mu_B$ ) is very close to results of neutron diffraction experiments.

On the other hand, in  $\text{BiFeO}_3$  compound the GGA DFT calculations revealed that the chemical bonding is predominantly of an ionic character with partial covalent components of the Bi–O and Fe–O bonds. For purely ionic bonding the spatial distribution of the charge would be purely spherical near the Bi, Fe, and O ions with keeping of an ideal perovskite structure. A covalent bonding facilitates stabilization of the structural distortions, which favours formation of a ferroelectric phase in  $\text{BiFeO}_3$ . In particular, hybridization of *s*, *p*-states of Bi with 2*p*-states of oxygen leads to a distinct spatial anisotropy of the charge density distribution and to an asymmetry in charge transfer in Bi–O bonds, which presumably causes ferroelectric polarization in  $\text{BiFeO}_3$ . On the other hand, hybridization of Fe(*d*)- and O(*p*)-states leads to substantial spin polarization in the AFM *G*-phase and to distortion and turning of the  $\text{FeO}_6$  octahedra. This hybridization reduces the value of magnetic moment of free  $\text{Fe}^{3+}$  ion to  $M_{\text{Fe}} \simeq 3.7\mu_B$ , and it is also responsible for spin polarization of electronic states of oxygen ions, providing the noticeable magnetic moment  $M_{\text{O}} \simeq 0.1\mu_B$  for each O ion.

The electronic structures of hexagonal strontium ferrites  $\text{SrFe}_{12}\text{O}_{19}$  and  $\text{SrCoTiFe}_{10}\text{O}_{19}$  were also calculated based on the generalized gradient approximation of DFT. However, the GGA+ $U$  method has been employed to improve the description of localized 3*d*-electrons, and to reproduce the insulating ground states of these compounds, with the energy gaps about 1 eV. Resultantly, the calculated magnetic moments of 3*d*-atoms are notably lower than the high spin values of the moments of free  $\text{Fe}^{3+}$  and  $\text{Co}^{2+}$  ions. In fact these moments are reduced in the crystal field environment, and the total magnetic moment is partly distributed among neighbouring oxygen ions. The total magnetic moment of ferrimagnetic  $\text{SrCoTiFe}_{10}\text{O}_{19}$  depends on the particular sites occupancy with substitution of  $\text{Fe}^{3+}$  ions by  $\text{Co}^{2+}$  and  $\text{Ti}^{4+}$ .

The results of the present work indicate that theoretical analysis of electronic structures of iron-based compounds with group VI elements (chalcogenides and oxygen) by means of GGA and GGA+ $U$  DFT calculations provides avenue to explore peculiar magnetic properties of different systems with strongly correlated electrons.

This includes superconductors with AFM ordering, various multiferroics, and strong ferrimagnets.

This work was supported by the Russian-Ukrainian RFBR-NASU project 78-02-14, and was performed using computational facilities of grid-cluster ILTPE B. Verkin Institute for Low Temperature Physics and Engineering of the National Academy of Sciences of Ukraine.

---

\* Electronic address: grechnev@ilt.kharkov.ua

- [1] Y. Mizuguchi and Y. Takano, *J. Phys. Soc. Jpn.* **79**, 102001 (2010) doi:10.1143/JPSJ.79.102001.
- [2] A. Martinelli, A. Palenzona, M. Tropeano, C. Ferdeghini, M. Putti, M.R. Cimberle, T.D. Nguyen, M. Afronte, and C. Ritter, *Phys. Rev. B* **81**, 094115 (2010) doi:10.1103/PhysRevB.81.094115
- [3] R. Viennois, E. Giannini, D. van der Marel, and R. Černý, *J. Solid State Chem.* **183**, 769 (2010) doi:10.1016/j.jssc.2010.01.024
- [4] S. Li, C. de la Cruz, Q. Huang, Y. Chen, J.W. Lynn, J. Hu, Y.-L. Huang, F.-C. Hsu, K.-W. Yeh, M.-K. Wu, and P. Dai, *Phys. Rev. B* **79**, 054503 (2009) doi:10.1103/PhysRevB.79.054503
- [5] G.E. Grechnev, A.S. Panfilov, A.V. Fedorchenko, V.A. Desnenko, S.L. Gnatchenko, V. Tsurkan, J. Deisenhofer, A. Loidl, D.A. Chareev, O.S. Volkova, A.N. Vasiliev, *J. Magn. Magn. Mater.* **324**, 3460 (2012) doi:10.1016/j.jmmm.2012.02.065
- [6] X. Chen, P. Dai, D. Feng, T. Xiang, and F.-C. Zhang, *National Science Review* **1** 371 (2014). doi:10.1093/nsr/nwu007
- [7] G. Catalan and J.F. Scott, *Adv. Mater.* **21**, 2463 (2009). doi:10.1002/adma.200802849
- [8] K.F. Wang, J.-M. Liu, and Z.F. Ren, *Adv. Physics* **58**, 321 (2009). doi:10.1080/00018730902920554
- [9] Gerald F. Dionne, *Magnetic oxides. Springer Verlag, Heidelberg*, 466p. (2009). doi:10.1007/978-1-4419-0054-8
- [10] P. Novak, K. Knizek, M. Kupferling, R. Grossinger, and M.W. Pieper, *Eur. Phys. J B* **43**, 509 (2005). doi:10.1140/epjb/e2005-00084-8
- [11] P. Novak and J. Ruzs, *Phys. Rev. B* **71**, 184433 (2005). doi:10.1103/PhysRevB.71.184433
- [12] R.C. Pullar, *Prog. Mater. Sci.* **57**, 1191 (2012). doi:10.1016/j.pmatsci.2012.04.001
- [13] L.S.I. Liyanage, S. Kim, Y.-K. Hong, J.-H. Park, S.C. Erwin, and S.-G. Kim, *J. Magn. Magn. Mater.* **348**, 75 (2013). doi:10.1016/j.jmmm.2013.08.006
- [14] K. Ebnabbasi, M. Mohebbi, and C. Vittoria, *J. Appl. Phys.* **113** 17C703 (2013). doi:10.1063/1.4793606
- [15] M. Feng, B. Shao, Y. Lu, and X. Zuo, *J. Appl. Phys.* **115** 17D908 (2014). doi:10.1063/1.4865886
- [16] G.E. Grechnev, *Low Temp. Phys.* **35**, 638 (2009). doi:10.1063/1.3224723.
- [17] J.M. Wills, M. Alouani, P. Andersson, A. Delin, O. Eriksson, A. Grechnev, Full-Potential Electronic Structure Method. Energy and Force Calculations with Density Functional and Dynamical Mean Field Theory. *Springer Verlag, Heidelberg*, 200p. (2010). doi:10.1007/978-3-642-15144-6
- [18] <http://fplmto-rspt.org/>
- [19] <http://elk.sourceforge.net/>
- [20] J.P. Perdew, K. Burke, and M. Ernzerhof, *Phys. Rev. Lett.* **77**, 3865 (1996). doi:10.1103/PhysRevLett.77.3865
- [21] A. Grechnev, R. Ahuja, and O. Eriksson, *J. Phys.: Condens. Matter* **15**, 7751 (2003). doi:10.1088/0953-8984/16/29/015
- [22] A. Subedi, L. Zhang, D.J. Singh, and M.H. Du, *Phys. Rev. B* **78**, 134514 (2008). doi:10.1103/PhysRevB.78.134514
- [23] Y. Liu, R.K. Kremer, and C.T. Lin, *Supercond. Sci. Technol.* **24**, 035012 (2011) doi:10.1088/0953-2048/24/3/035012
- [24] J.B. Neaton, C. Ederer, U.V. Waghmare, N.A. Spaldin, and K.M. Rabe, *Phys. Rev. B* **71**, 014113 (2005). doi:10.1103/PhysRevB.71.014113
- [25] S.J. Clark and J. Robertson, *Appl. Phys. Lett.* **90** 132903 (2007). doi:10.1063/1.2716868
- [26] J.A. McLeod, Z.V. Pchelkina, L.D. Finkelstein, E.Z. Kurmaev, R.G. Wilks, A. Moewes, I.V. Solovyev, A.A. Belik, and E. Takayama-Muromachi, *Phys. Rev. B* **81**, 144103 (2010). doi:10.1103/PhysRevB.81.144103
- [27] I. Sosnowska, W. Schafer, W. Kockelmann, K.H. Andersen, and I.O. Troyanchuk, *Appl. Phys. A* **74**, [Suppl.], S1040 (2002). doi:10.1007/s003390201604
- [28] A.I. Liechtenstein, V.I. Anisimov, and J. Zaanen, *Phys. Rev. B* **52**, 5467 (1995). doi:10.1103/PhysRevB.52.R5467